Quantification of organic aerosol and brown carbon evolution in fresh wildfire plumes

Brett B. Palm[a,1], Qiaoyun Peng[a], Carley D. Fredrickson[a], Ben H. Lee[a], Lauren A. Garofalo[b], Matson A. Pothier[b], Sonia M. Kreidenweis[c], Delphine K. Farmer[b], Rudra P. Pokhrel[d,2], Yingjie Shen[d], Shane M. Murphy[d], Wade Permar[e], Lu Hu[e], Teresa L. Campos[f], Samuel R. Hall[f], Kirk Ullmann[f], Xuan Zhang[f,3], Frank Flocke[f], Emily V. Fischer[c], and Joel A. Thornton[a,1]

[a]Department of Atmospheric Sciences, University of Washington, Seattle, WA 98195; [b]Department of Chemistry, Colorado State University, Fort Collins, CO 80523; [c]Department of Atmospheric Science, Colorado State University, Fort Collins, CO 80523; [d]Department of Atmospheric Science, University of Wyoming, Laramie, WY 82071; [e]Department of Chemistry and Biochemistry, University of Montana, Missoula, MT 59812; and [f]Atmospheric Chemistry Observations and Modeling Laboratory, National Center for Atmospheric Research, Boulder, CO 80301

Edited by John H. Seinfeld, California Institute of Technology, Pasadena, CA, and approved September 29, 2020 (received for review June 15, 2020)

The evolution of organic aerosol (OA) and brown carbon (BrC) in wildfire plumes, including the relative contributions of primary versus secondary sources, has been uncertain in part because of limited knowledge of the precursor emissions and the chemical environment of smoke plumes. We made airborne measurements of a suite of reactive trace gases, particle composition, and optical properties in fresh western US wildfire smoke in July through August 2018. We use these observations to quantify primary versus secondary sources of biomass-burning OA (BBPOA versus BBSOA) and BrC in wildfire plumes. When a daytime wildfire plume dilutes by a factor of 5 to 10, we estimate that up to one-third of the primary OA has evaporated and subsequently reacted to form BBSOA with near unit yield. The reactions of measured BBSOA precursors contribute only 13 ± 3% of the total BBSOA source, with evaporated BBPOA comprising the rest. We find that oxidation of phenolic compounds contributes the majority of BBSOA from emitted vapors. The corresponding particulate nitrophenolic compounds are estimated to explain 29 ± 15% of average BrC light absorption at 405 nm (BrC Abs_{405}) measured in the first few hours of plume evolution, despite accounting for just 4 ± 2% of average OA mass. These measurements provide quantitative constraints on the role of dilution-driven evaporation of OA and subsequent radical-driven oxidation on the fate of biomass-burning OA and BrC in daytime wildfire plumes and point to the need to understand how processing of nighttime emissions differs.

biomass burning | secondary organic aerosol | brown carbon | phenolic compounds | aircraft measurements

Biomass burning (BB) is a major global source of atmospheric trace gases (1, 2), fixed nitrogen (3–6), and primary organic carbonaceous fine particles, known as BB organic aerosol (BBOA) (7). These emissions and their subsequent atmospheric transformations play a major role in affecting air quality, atmospheric composition, and climate.

Questions remain about the magnitude of BBOA emissions and evolution, particularly the relative contributions that are primary, i.e., directly emitted (BBPOA), versus secondary, i.e., formed from gas-to-particle conversion following the oxidation of emitted vapors (BBSOA). Measurements of laboratory burns of individual or ensemble biomass fuel types have suggested that the BBSOA source could be anywhere from negligible to twice as large as the BBPOA source (8–11). On the other hand, field measurements have generally suggested little to no net change in BBOA in wildfire plumes (12–17). A leading hypothesis is that any BBSOA formation is offset by evaporation of BBPOA due to dilution-driven repartitioning of semivolatile components to the gas phase, making the magnitude of each difficult to discern (e.g., refs. 12, 14, 16–19). Recent plume modeling has investigated this behavior in detail, although the magnitudes of evaporation and BBSOA formation remain unclear due to limited observational constraints (20, 21). This hypothesis is uncertain in part because previous wildfire studies of BBSOA often did not include all potentially important precursor gases such as phenolic compounds. Laboratory studies have indicated that oxygenated aromatic compounds (i.e., phenolic compounds) are a large and often dominant source of BBSOA in BB smoke, although other sources including reduced aromatic compounds, biogenic compounds, and heterocyclic compounds (e.g., furans) can also be major BBSOA sources (11, 22–25).

BB is also considered a major contributor to atmospheric brown carbon aerosol (BrC), which absorbs solar radiation and thus acts similarly to black carbon (BC) to potentially warm and stabilize the atmosphere (26–28). The lifetime of BrC and the importance of secondary BrC (sBrC) formation both remain uncertain. Phenolic compound emissions from wildfires are thought to be potentially important precursors for sBrC formation given their propensity to form light-absorbing nitroaromatics upon oxidation

Significance

Wildfire emissions in the western United States have had increasingly larger impacts on air quality, health, and climate forcing in recent decades. However, our understanding of how wildfire plume composition evolves remains incomplete. Particularly, the evolution of carbonaceous material, including fine particle mass ($PM_{2.5}$) and light-absorbing brown carbon, has remained elusive because of limited knowledge about the interplay between primary emissions and subsequent chemical and physical transformations that convert material between vapors and particles. Using a comprehensive analysis of in situ wildfire smoke measurements in combination with simulation chamber experiments, we quantitatively assess primary versus secondary organic particulate matter and brown carbon light absorption in authentic wildfires plumes. These results improve our fundamental knowledge of wildfire plume composition and evolution.

Author contributions: J.A.T. designed research; B.B.P., Q.P., C.D.F., B.H.L., L.A.G., M.A.P., S.M.K., D.K.F., R.P.P., Y.S., S.M.M., W.P., L.H., T.L.C., S.R.H., K.U., X.Z., F.F., E.V.F., and J.A.T. performed research; B.B.P. analyzed data; and B.B.P. wrote the paper.

The authors declare no competing interest.

This article is a PNAS Direct Submission.

[1]To whom correspondence may be addressed. Email: bbpalm@uw.edu or joelt@uw.edu.

[2]Present address: Department of Physics, North Carolina Agricultural and Technical State University, Greensboro, NC 27411.

[3]Present address: Department of Life and Environmental Sciences, University of California, Merced, CA 95343.

This article contains supporting information online at https://www.pnas.org/lookup/suppl/doi:10.1073/pnas.2012218117/-/DCSupplemental.

First published November 4, 2020.

in the nitrogen oxide-rich fire plumes (29, 30). Phenolic compound oxidation products, including nitrophenolic compounds, have been estimated to account for up to approximately one-third to one-half of BrC light absorption for regions impacted by residential wood smoke and agricultural BB (31–34). Similar to BBSOA, field measurements of BrC absorption have generally shown little or no secondary formation in wildfire plumes, instead showing mostly decay with lifetimes from 9 h up to more than 1 d (16, 35). Understanding the controls on BrC and its secondary source can enable better predictions of its contribution and fate as wildfire smoke ages.

We introduce a method for quantifying the effects of secondary formation versus dilution-driven evaporation for both total organic aerosol (OA) and BrC evolution in wildfire plumes. OA was measured using a high-resolution time-of-flight aerosol mass spectrometer (AMS), and BrC was quantified using a photoacoustic absorption spectrometer (PAS). To address the relative contributions to BBSOA formation from either primary emitted precursors (e.g., phenolic compounds) versus evaporated BBPOA, we quantified all major secondary OA (SOA) precursor gases measured using an iodide-adduct, high-resolution time-of-flight chemical ionization mass spectrometer (I^- CIMS) and a proton-transfer reaction time-of-flight mass spectrometer (PTR-ToF-MS) in authentic wildfire smoke plumes during the airborne Western Wildfire Experiment for Cloud Chemistry, Aerosol Absorption, and Nitrogen (WE-CAN) field campaign. The WE-CAN project deployed a research aircraft across the western United States between 22 July and 13 September 2018 to sample wildfire smoke during the first several hours of atmospheric evolution. To investigate the contributions of particulate nitrophenolic compounds to BrC Abs_{405}, environmental chamber experiments were performed at the National Center for Atmospheric Research (NCAR) chamber facility in May/June 2019 as part of the Monoterpene and Oxygenated aromatic Oxidation at Night and under LIGHTs (MOONLIGHT) campaign. These experiments simulated phenolic compound oxidation chemistry in fresh wildfire plumes. Through a combined analysis of these data, we characterize the importance of phenolic compound emissions and nitrophenolic oxidation products as potential contributors to BBSOA and sBrC, compared to the sources from evaporated BBPOA vapors.

Insights into Dilution-Driven BBPOA Evaporation and BBSOA Formation

The relative contributions of dilution-driven evaporation of BBPOA versus BBSOA formation from either primary emitted gases or the evaporated BBPOA have remained elusive in wildfire studies. Many studies have hypothesized a serendipitous balance between the two, leading to little to no net change in BBOA relative to carbon monoxide (CO) (considered a conserved tracer of dilution) as fire plumes age, including from WE-CAN (17) and others (e.g., refs. 12, 14, 16, 18, 19). The relative contributions of primary and secondary sources to BrC evolution in wildfire plumes have been even less clear (16, 29, 35–37). To evaluate the various processes, we use WE-CAN observations made in fresh wildfire plumes at different extents of plume dilution and chemical aging, as summarized in Fig. 1.

We evaluate the changes in BBOA and BrC light absorption at 405 nm (BrC Abs_{405}) using the normalized excess mixing ratio (NEMR) concept, where the difference between the measured in-plume and out-of-plume ("background") mixing ratio (defined as enhancement) is normalized to that of CO (called CO enhancement; *SI Appendix*, Eq. **S1**). We then use the difference in the OA or BrC Abs_{405} NEMR, i.e., ΔNEMR, within a smoke plume between any given transect and that of the densest part of the plume, which is defined as the plume transect with the highest average CO enhancement. The densest plume transect through each smoke plume was always one of the physically closest transects to the fire source but not always the absolute closest, in part due to the challenges of navigating the aircraft through the central portions of the plumes in the fire's vicinity. Plume density varies significantly in the vertical, so the assignment of the densest transect depends as much on the vertical location of the aircraft as well as the horizontal proximity to the fire. The densest (and physically freshest) transects were typically sampled at a physical age of ~20 to 50 min. Any secondary chemistry that occurs in the short time between emission and the densest transect cannot be accounted for with the observational analysis here but is expected to be relatively minor because of the short reaction time. We thus operationally define the OA sampled in the densest plume transect as consisting only of BBPOA, while any OA that is determined to be formed due to oxidative plume aging, we label as BBSOA. Our estimates of total BBSOA concentrations may be underestimated due to these assumptions.

The effects of plume dilution can then be investigated by comparing these ΔNEMR values as a function of an observationally constrained plume dilution factor, defined as the ratio of the CO enhancement in the densest part of a sampled plume to the CO enhancement in each of the other transects of that plume. We use the average CO enhancements across each plume transect to smooth over small-scale plume structures. The dilution factor accounts for dilution due to eddy mixing in both the horizontal and vertical directions but does not separate between them. For example, the dilution factor on the edge of a plume near the fire could be equivalent or higher than that in the core of a plume sampled physically further downwind, despite the downwind plume having spent relatively more time in the atmosphere after emission. In other words, physical age and dilution factor are not necessarily correlated.

In the absence of oxidation chemistry, the ΔNEMR of OA and BrC Abs_{405} in a diluting plume are expected to either be invariant or decrease with further dilution as intermediate-volatility organic compounds (IVOCs) and semivolatile organic compounds (SVOCs) evaporate to maintain equilibrium with decreasing vapor concentrations (38–40) or chromophores become photobleached (16, 37, 41, 42). However, emissions of radical precursors such as nitrous acid (HONO) and the presence of increasing solar radiation as the plume dilutes promote oxidation of vapors that were coemitted with BBPOA or that result from BBPOA evaporation, causing potential BBSOA and sBrC formation. The extent of potential BBSOA chemistry can also be described quantitatively using measured reactive losses (i.e., dilution-corrected decreases) of known BBSOA precursors. Observations of these quantities across a diverse range of wildfire plumes provide the opportunity to examine the competing roles of dilution and potential BBSOA- and sBrC-formation chemistry. In particular, the WE-CAN sampling of aged and fresh plumes during midday with active oxidation chemistry as well as plumes that were emitted and sampled closer to sunset, when the rate of oxidation chemistry had slowed, provided a unique set of observational constraints from rarely probed fire plume conditions.

The quantitative relationships between these three quantities, Δ(OA NEMR) or Δ(BrC Abs_{405} NEMR), extent of BBSOA-formation chemistry, and plume dilution across multiple wildfire plumes are summarized in Fig. 1 *B* and *C*. We separate the observations into three broad categories of dilution, ranging between dilution factors of 1 to 3, 3 to 6, or 6 to 13 relative to the densest sampled portion of each fire plume (referred to as low, medium, and high dilution), where the larger the dilution factor, the more dilute the plume has become. For each of these categories, we plot the observed ΔNEMR versus the fraction of measured phenolic compound vapors (described below in *Evaporated BBPOA Dominates among BBSOA Sources*) that have reacted relative to the densest sampled portion of the plume. That fraction is an approximate measure of the chemical age of the plumes and thus is a better proxy for the extent of BBSOA-formation

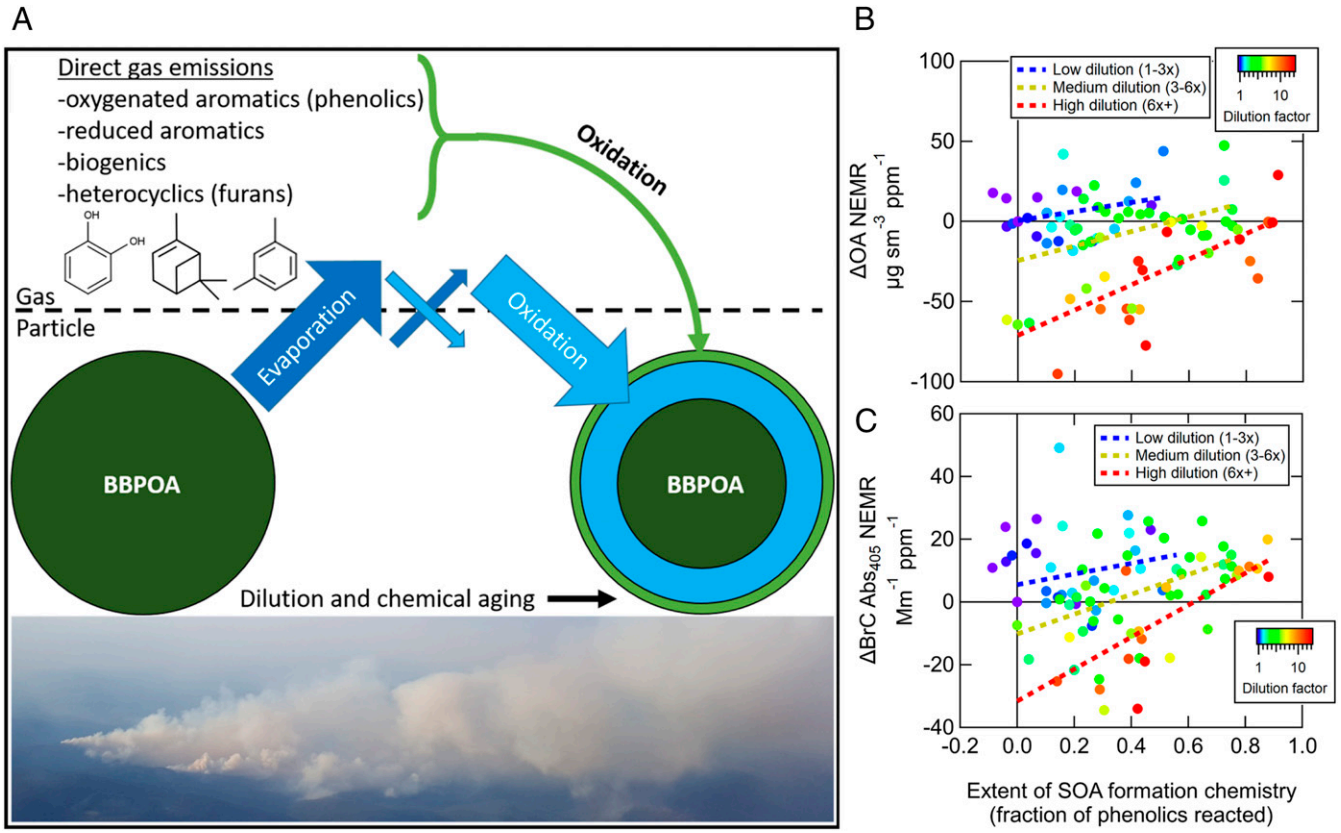

Fig. 1. (*A*) Observationally constrained schematic illustrating the dominance of evaporated BBPOA as a source of BBSOA formation as wildfire plumes physically and chemically age. (*B* and *C*) Difference in OA NEMR (*B*) and difference in BrC absorption NEMR (*C*) between each plume transect and the densest plume transect of its respective fire, as a function of reacted amount of phenolics. Data are colored by dilution factor, accounting for dilution during downwind advection as well as from vertical or horizontal distance from plume core. Evaporation of OA and BrC upon dilution is balanced by secondary formation from phenolics (and other precursor gases).

chemistry than the physical plume age. Both the chemical age and the dilution rate in each plume will proceed nonlinearly relative to physical age, and the relative rates will also be variable across different plumes, as variables such as time of day and fire size change. The use of this chemical age proxy is based on the assumption that SOA precursors, whether directly emitted as gases or formed as evaporated primary OA (POA), will have similar reactivities toward hydroxyl (OH) radicals and other oxidants as emitted phenolic compounds. The processes of dilution and SOA formation shown in Fig. 1 occurred rapidly within the first few hours of physical age.

The dilution of the plume leads to a certain amount of net evaporation of OA and BrC or other losses (e.g., photobleaching of chromophores), and thus ΔNEMR < 0 when dilution has occurred but BBSOA-formation chemistry has not proceeded. However, as the extent of BBSOA-formation chemistry increases, the ΔNEMR in all dilution regimes increase. Trend lines of the ΔNEMR versus extent of potential BBSOA formation are fit for each category of dilution using least orthogonal distance regression (uncertainties quoted here are ±1 SD). In the absence of BBSOA-formation chemistry, the *y* intercepts of the trend lines define the magnitude of BBPOA or BrC Abs_{405} evaporation. BBSOA that formed from oxidation in the plume prior to sampling the densest transect could also be evaporating, but evaporation of BBPOA is likely the dominant process since BBSOA is expected to be a minor component in the densest transects. Little to no evaporation is measured with low dilution. A medium dilution factor causes evaporation of ∼25 ± 9 micrograms per standard cubic meter per part per million ($\mu g\ sm^{-3}\ ppm^{-1}$) OA and 10 ± 5 per megameter (Mm^{-1}) ppm^{-1} BrC Abs_{405}, while a high dilution factor causes evaporation of 70 ± 9 $\mu g\ sm^{-3}\ ppm^{-1}$ OA and 32 ± 7 $Mm^{-1}\ ppm^{-1}$ BrC Abs_{405}. With a typical OA emission ratio (ER) of 250 ± 30 $\mu g\ sm^{-3}\ ppm^{-1}$ (17), this corresponds to evaporation of 10 ± 4% and 28 ± 5% of total BBPOA. For BrC Abs_{405}, these values similarly correspond to evaporation or other losses of 8 ± 4% and 26 ± 8% based upon a typical ER of 125 ± 30 $Mm^{-1}\ ppm^{-1}$.

Superimposed on top of evaporation are the consistent trends of increasing ΔNEMR values with increasing extent of potential BBSOA-formation chemistry, indicated by the positive slopes of the trend lines. The magnitude of change in ΔNEMR OA and BrC Abs_{405} between no BBSOA-formation chemistry and the full measured extent of BBSOA-formation chemistry then defines the magnitude of BBSOA and sBrC Abs_{405} formation from all sources and, while >0 in all dilution regimes, varies as a function of dilution factor. With a low dilution factor, while a smaller range of chemical processing was sampled, the slope is also smaller suggesting relatively suppressed BBSOA formation. With medium dilution, the observed change in ΔNEMR of OA and BrC Abs_{405} at the full extent of BBSOA-formation chemistry requires production of ∼35 ± 18 $\mu g\ sm^{-3}\ ppm^{-1}$ BBSOA and 25 ± 10 $Mm^{-1}\ ppm^{-1}$ sBrC Abs_{405}. At high dilution, ∼75 ± 16 $\mu g\ sm^{-3}\ ppm^{-1}$ BBSOA formation and 45 ± 12 $Mm^{-1}\ ppm^{-1}$ sBrC Abs_{405} formation are required to explain the observed trends.

Importantly, the medium and high dilution trend lines reach amounts of ΔOA NEMR and ΔBrC Abs_{405} NEMR at the higher extent of potential BBSOA formation that are consistent with there being little to no net change in total OA or BrC Abs_{405} with

plume aging, at least over the first ~6 h of aging after emission that were primarily sampled during WE-CAN flights. Thus, we illustrate a quantitative separation of the processes leading to typically small observed changes in BBOA relative to CO as a function of plume age. Our observational analysis suggests that balance is achieved between dilution-driven evaporation (or other losses) and concurrent BBSOA and sBrC formation in wildfire plumes. When a typical western US wildfire plume has diluted by an average factor of ~10 (relative to the densest plumes sampled here), approximately one-third of total BBOA will have converted from BBPOA to BBSOA, which is consistent with the observed increase in OA oxidation state measured in these same plumes (17). Moreover, our observational insights support dynamic OA repartitioning and oxidation invoked in recent models of BBOA emission and evolution (20, 21).

The trend lines in Fig. 1 *B* and *C* emerge because the WE-CAN flights sampled a wide enough range of plume-transect conditions to fill in the Fig. 1 coordinates. The campaign-wide trends allow us to separate the effects of dilution-driven evaporation and BBSOA formation averaged over multiple fires. For practical sampling reasons, the data from transects of a single plume typically do not cover a broad enough extent to robustly determine such trends. In reality, both evaporation and BBSOA formation occur simultaneously in most plumes. In a typical midday plume with rapid photochemistry (i.e., many of the plumes sampled here and during previous campaigns), dilution-driven evaporation appears to be the rate-limiting step. SOA formation occurs rapidly after evaporation of BBPOA, causing observed ΔOA and ΔBrC Abs_{405} NEMRs to remain small as daytime plumes progress from low to high extent of BBSOA-formation chemistry and dilution simultaneously. Regardless of the specific path taken through the Fig. 1 coordinates (i.e., relative rates of dilution and BBSOA formation) for a given plume, our results suggest all of these western US wildfire plumes converge toward maintaining near-constant OA and BrC Abs_{405} NEMRs once both dilution and BBSOA-formation chemistry have occurred.

The above analysis suggests that BBSOA and sBrC formation equivalent to 5 to 30% of BBPOA and BrC emissions occurred over the extent of chemical aging in wildfire plumes sampled during WE-CAN. In what follows, we evaluate the extent to which simultaneous observations of a suite of trace gases and particulate components commonly identified as the dominant BBSOA and sBrC precursors explain these extents of BBSOA and sBrC formation.

Evaporated BBPOA Dominates among BBSOA Sources

Several recent studies have combined laboratory measurements with modeling to investigate the sources of BBSOA from oxidation of smoke from various sources (11, 22–25). Generally, the BBSOA precursors fall into four main categories: oxygenated aromatics (i.e., phenolic compounds), reduced aromatics, biogenics, or heterocyclic compounds (e.g., furans). The emissions, and thus magnitude of BBSOA formation, from each category can depend on various parameters, including fuel type, fuel condition, and flaming versus smoldering burn conditions (e.g., refs. 2, 10, 43). The contributions of these categories in wildfire smoke are also uncertain, in large part due to a lack of measurements, especially for phenolic compounds. Here, we evaluate the ERs in wildfire smoke of compounds in each of the four categories using a combination of simultaneous, high-time resolution observations of volatile organic compounds (VOCs), IVOCs, and SVOCs measured with an I^- CIMS and a PTR-ToF-MS. Instrument descriptions are provided in *SI Appendix*.

We first characterize several regimes of reactive carbon in the gas phase of wildfire smoke plumes during WE-CAN as a function of physical plume aging. The physical age of each plume transect was estimated as the distance from the center of the plume transect to the estimated fire location, divided by the average wind speed measured throughout the plume. A representative mass spectrum from the I^- CIMS showing the difference and percentage change of a wide array of measured plume components upon aging of a fresh plume can be found in *SI Appendix*, Fig. S1 for the Taylor Creek fire plume sampled on 30 July 2018 and in *SI Appendix*, Fig. S2 for the Sharps fire plume sampled on 31 July 2018. The most prominent compounds in the spectrum were oxidized organic molecules containing five or fewer carbon atoms. Previous research has identified these compounds as likely to be small multifunctional organic compounds such as furans (22, 44) or derivatives thereof. Several phenolic compounds were also present in fresh smoke, although at relatively lower concentrations than many of the smaller oxidation products.

Fig. 2 illustrates the NEMR values as a function of physical age after emission for several groups of compounds in the Taylor Creek plume. As in *SI Appendix*, Figs. S1 and S2, nearly all of the compounds that depleted with aging in the I^- CIMS were likely phenolic in nature, joined also by several likely furans and HONO (45). Several compounds measured by the PTR-ToF-MS (including monoterpenes, reduced aromatics, and several furans) also followed this behavior, suggesting direct emissions followed by rapid reaction early in the plume evolution for the compounds shown in Fig. 2*A*. Other compounds (e.g., nitrophenolics) exhibit behavior suggesting they were initially formed through oxidation chemistry of emitted precursors (or from evaporation of BBPOA) and were then reacted away or condensed into the particle phase once their precursor sources had been depleted (Fig. 2*C*). Finally, another group of mostly smaller compounds (one to five carbon atoms) were found in persistently increasing concentrations as the products of oxidative plume chemistry (Fig. 2*B*). These compounds likely include furan oxidation products and fragmentation products from compounds with six or more carbon atoms. *SI Appendix*, Figs. S1 and S2 illustrate that while variability is seen in the behavior of individual compounds across different fires, the broader trends outlined in Fig. 2 are consistent for all fire plumes. Similar trends are also seen in the PTR-ToF-MS spectrum for both fire plumes (*SI Appendix*, Fig. S3). For reference, the Taylor Creek plume is highlighted among all plume transects executed during WE-CAN in Fig. 2*D*.

For the reactive, directly emitted species in Fig. 2*A*, the NEMR as a plume ages will depend on the extent of oxidation or other chemical transformation that has occurred between time of emission and time of sampling. For the fastest reacting species, such as some phenolic compounds, the lifetime with respect to oxidation can be as little as tens of minutes or less, depending on conditions. To illustrate this reactivity for several major directly emitted species across all four major emission categories, average NEMRs across each plume transect during the campaign were plotted as a function of estimated physical plume age in Fig. 3. Similar figures for all other species with obvious behavior suggesting direct emissions and rapid decay are shown in *SI Appendix*, Figs. S4 and S5. For the fastest reacting species $C_6H_6O_2$ (likely catechol) and $C_7H_8O_2$ (likely methyl catechol), nearly all of the compound had reacted away within the first 60 min or less of plume aging. Most other compounds typically reacted away within the first 100 to 200 min. The slowest-reacting compounds, such as C_6H_6 (benzene) and C_7H_8 (toluene), typically remained to longer ages than were sampled during WE-CAN (*SI Appendix*, Fig. S5).

We assume the reactive loss of these species is controlled by plume concentrations of OH, which in turn is likely produced predominantly by HONO photolysis in these plumes (2, 15, 44–47). Consistent with this assumption, much of the scatter of NEMR values in Fig. 3 (and *SI Appendix*, Figs. S4 and S5) is explained by the measured photolysis frequency of HONO (j_{HONO}), which is a proxy for the amount of sunlight available to drive photochemistry. During daytime when j_{HONO} in plumes

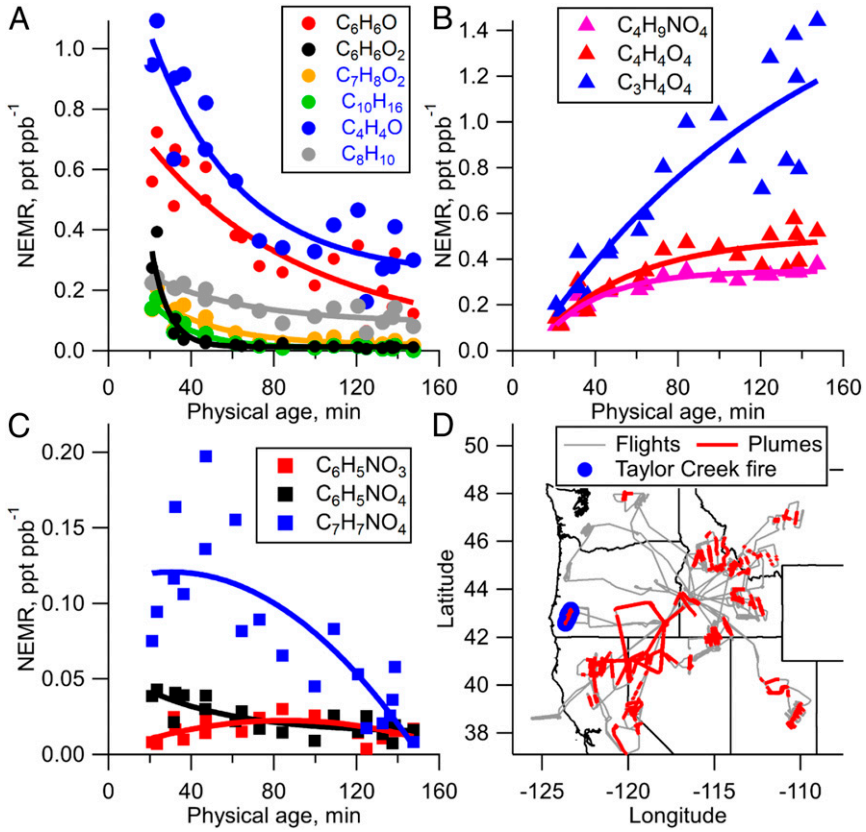

Fig. 2. (*A–C*) NEMR of several groups of compounds with differing behaviors in the Taylor Creek plume, including examples of oxygenated aromatic (phenolic), reduced aromatic, biogenic, and heterocyclic (furans) compounds that were predominantly direct emissions and were subsequently reacted away (*A*); compounds exhibiting net production due to oxidation chemistry (*B*); and compounds that were formed as oxidation products and were also subsequently reacted away (or condensed into the particle phase) (*C*). *D* illustrates all flight tracks and discrete plume transects, with the Taylor Creek plume in Southern Oregon highlighted. Exponential or polynomial fits are shown for each compound to guide the eye. Compounds with black text indicate an I^- CIMS measurement, while blue text indicates a PTR-TOF-MS measurement.

was large (1×10^{-3} to 2×10^{-3} s^{-1}; HONO photolysis lifetime of 8 to 17 min), OH concentrations were likely to be relatively higher early in the plume evolution, causing most of the compounds to react away within the first 1 to 2 h following emission. During the several plumes that were sampled as the sun was setting, j_{HONO} decreased to 1×10^{-4} to 5×10^{-4} s^{-1} (HONO photolysis lifetimes of 33 to 167 min), leading to much lower OH production (relative to midday plumes), allowing many compounds to persist within physically older plumes. HONO also followed this same pattern, as presented in ref. 45 and shown in the *SI Appendix*, Fig. S6 for reference. Nitrate (NO_3) radicals may have also contributed to the decay of phenolics, especially when j_{HONO} was relatively low, but contributions were likely minor during most daytime plumes.

For all of the compounds shown in Fig. 3 as well as other emissions shown in the *SI Appendix*, Figs. S4 and S5, we calculated ERs in order to estimate the magnitude of all directly emitted BBSOA sources quantified using the available techniques. Since many of these compounds react rapidly after emission, we estimated their ERs as the average of the measured NEMRs in plume transects where both rate of and time allowed for photochemistry were minimized, in order to derive the best estimate of ER at the fire source. Specifically, we used NEMRs from the closest plume transect of each fire that also had average j_{HONO} $<5 \times 10^{-4}$ s^{-1} and was sampled <100 min after emission (except for $C_6H_6O_2$ and $C_7H_8O_2$ measured with I^- CIMS, for which a 50-min threshold was used to account for their faster reactivity). Several of the highest estimated ERs were 1.8 parts per trillion per part per billion (ppt ppb^{-1}) for C_4H_4O, 1.7 ppt ppb^{-1} for both C_6H_6 and $C_5H_4O_2$, 1.1 and 0.42 ppt ppb^{-1} for C_6H_6O and $C_6H_6O_2$ measured using I^- CIMS (likely phenol and catechol/benzenediols), and 0.68 ppt ppb^{-1} for $C_{10}H_{16}$. Even with this restrictive method of estimating ERs, the lifetimes of some of these species were of the same order as the shortest physical plume ages that were sampled, due mainly to practical restrictions of flying close to wildfires. Therefore, the ERs presented here may be underestimated, perhaps by as much as a factor of 2, and the uncertainties are larger for the faster reacting compounds. Generally, the ER values reported here (*SI Appendix*, Table S1) range from 0.1 to 2 ppt ppb^{-1} and are of the same order as previously reported values for laboratory measurements of BB, which themselves exhibit large variability (e.g., refs. 44, 48, 49). Indeed, laboratory BB experiments may not be directly comparable to field measurements, due to differences in fuel mixtures, fuel moisture content, relative contributions of flaming versus smoldering versus distillation emissions, etc.

Using these ERs, we calculated a bottom-up estimate of total expected BBSOA formation from all major measured BBSOA precursor gas emissions. For each precursor, we calculate a potential BBSOA mass contribution using SOA yield values from the literature (*SI Appendix*, Table S2 and refs. therein), together with the observed depletion of the precursor over the range of plume ages sampled during WE-CAN. With this method, we estimate that typical western US wildfire plumes produce a net 9.8 ± 1.4 μg sm^{-3} ppm^{-1} BBSOA from the near-field oxidation of vapors observed in typical daytime plumes. This accounts for

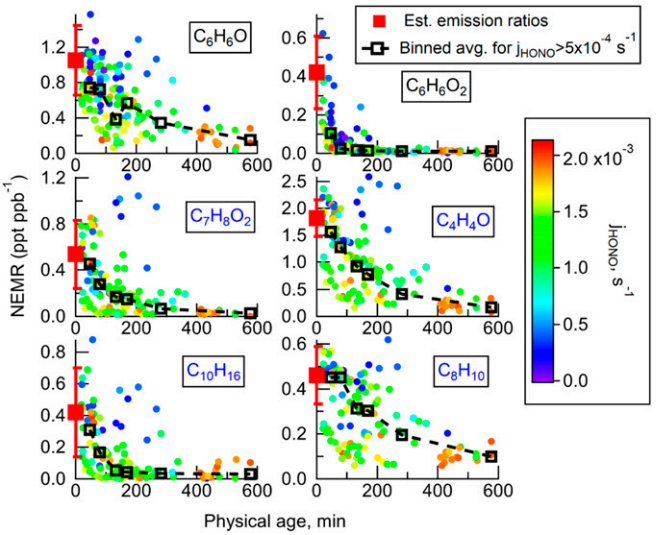

Fig. 3. ERs and NEMRs of several compounds, including examples of oxygenated aromatic (phenolic), reduced aromatic, biogenic, and heterocyclic (i.e., furans) compounds, as a function of estimated physical age of the plume. Binned averages of the NEMR data collected during daytime (j_{HONO} >5 × 10^{-4} s^{-1}) are shown as a guide. NEMR data are also colored by j_{HONO}, illustrating the increased chemical lifetimes due to expected decreases in OH concentrations as j_{HONO} decreased late in the day. Error bars on ER values are the SDs of the data from which the ER average was estimated. Compounds with black text indicate an I$^-$ CIMS measurement, while blue text indicates a PTR-TOF-MS measurement.

13 ± 3% of the total 75 ± 16 μg sm^{-3} ppm^{-1} estimated BBSOA formation. In fractional terms, phenolic compounds were by far the largest measured source of BBSOA from directly emitted gases at 56%, followed by heterocyclic compounds at 18%, aromatic hydrocarbons at 17%, and biogenic compounds at 8% (Fig. 4). Our observations of a suite of phenolic compounds in fresh daytime wildfire plumes allow for this direct comparison against other common BBSOA precursors and suggest that the BBSOA formed may be light-absorbing and thus contribute to sBrC, as we discuss in *Phenolic BBSOA and BrC Light Absorption*.

The BBSOA source estimate of 9.8 ± 1.4 μg sm^{-3} ppm^{-1} is conservative but still small compared to the measured range of 200 to 300 μg sm^{-3} ppm^{-1} total BBPOA (17). There are of course significant uncertainties in this bottom-up BBSOA estimate, stemming both from potential low biases in laboratory determined SOA yields with associated vapor wall loss and also unmeasured or unquantified vapors in the wildfire plumes. Moreover, as noted above, we may underestimate the ER of the most reactive BBSOA precursors, especially the phenolic compounds that make up the largest portion of the estimate. Consensus suggests that SOA yields from chamber experiments can be biased low by a factor of 2 to 4 in some cases (20, 50), and the previous laboratory BB studies with more comprehensive speciation and quantification of BB emissions of VOCs and IVOCs suggest the categories of precursors we quantify here are the dominant BBSOA contributors. If we propagate the bottom-up estimate in the *SI Appendix*, Table S2 but multiply the SOA yields by a factor of 2, we would estimate 19.6 ± 2.8 μg sm^{-3} ppm^{-1}, or 26 ± 7% of the total. Therefore, even taking into account large potential low biases in SOA yields, we conclude that BBSOA formation from gas-phase oxidation of vapors emitted at the fire source plays a minor role in determining total BBOA concentrations and properties. Indeed, even if a 100% SOA yield were applied to all BBSOA precursors in *SI Appendix*, Table S2, including furans, which is unlikely, these precursors could account for only 62 ± 14% of total 75 ± 16 μg sm^{-3} ppm^{-1} estimated BBSOA formation.

As this bottom-up estimate from direct gas-phase emissions only accounts for 9.8 ± 1.4 μg sm^{-3} ppm^{-1} BBSOA out of the total top-down maximum estimate of 75 ± 16 μg sm^{-3} ppm^{-1} in Fig. 1*A*, it follows that the remainder of that total (65.2 ± 16.1 μg sm^{-3} ppm^{-1}) is formed from subsequent oxidation of evaporated BBPOA with near unit SOA yield. Thus, evaporated BBPOA is shown here to be the dominant source of BBSOA in aged wildfire plumes, as illustrated schematically in Figs. 1*A* and 4. The specific identities of evaporated BBPOA compounds remains unclear, for several reasons. This subset of compounds will have relatively low O:C ratios, which is a class of compounds that tend not to cluster strongly enough with I$^-$ anions to be sensitively detected in the I$^-$ CIMS technique. These compounds are also likely IVOCs or SVOCs with relatively low volatility, which are not typically sampled well in short pulses with the PTR-ToF-MS technique due to inlet wall effects (51, 52). Lastly, and likely most significantly, the sum of evaporated BBPOA is likely spread over many compounds, each with relatively low concentrations maintained by a pseudo-steady state, where evaporation and oxidation with recondensation are approximately balanced, making detection and attribution difficult in a complex BB plume environment.

Phenolic BBSOA and BrC Light Absorption

As noted above, oxidation of phenolic compounds in the fresh wildfire plumes explains a substantial portion of inferred BBSOA. The related nitrophenolic products, which are known to contribute to BrC Abs$_{405}$, were also simultaneously speciated in the gas phase (*SI Appendix*, Fig. S7) and detected in the particle phase as part of total OA in these plumes. Similar to the trends for OA as a function of dilution factor and extent of reaction, BrC Abs$_{405}$ exhibited both dilution-driven loss and secondary formation (Fig. 1*C*). To investigate the contributions of nitrophenols to BBSOA and BrC, either as direct emissions or stemming from their in-plume oxidation, we conducted a series of laboratory chamber experiments probing oxidation of phenolic compounds and the resulting SOA formation and aerosol light absorption during the MOONLIGHT campaign (see *SI Appendix* for more details). Briefly, this campaign probed the OH and NO_3 radical oxidation of phenol, catechol, cresol, and guaiacol under high-nitrogen oxide conditions to mimic wildfire plumes. These experiments allowed direct connections between gas-phase phenolic compounds, their oxidation products, and the corresponding particle composition and light-absorbing properties.

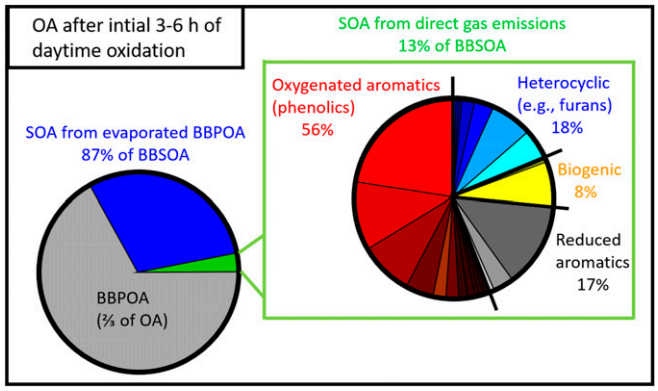

Fig. 4. Relative contributions of BBPOA versus BBSOA after initial rapid chemical aging (i.e., oxidation of most directly emitted SOA precursor gases) has completed. An observationally constrained bottom-up analysis indicates oxygenated aromatic compounds are the largest BBSOA source among directly emitted gases, but evaporated BBPOA dominates as a BBSOA source.

The major advance of this laboratory campaign was the connection of the magnitude of BrC Abs_{405}, measured using the PAS, with the concentrations of light-absorbing particulate nitrophenolic products. The nitrophenolic compounds were detected as part of total OA using an AMS, and they were detected as part of the speciated particulate molecular composition measurements made using a Filter Inlet for Gases and Aerosols (FIGAERO) coupled to the I^- CIMS (53). The I^- CIMS, AMS, and PAS were the same instruments used to generate observations shown in Figs. 1–3 during the WE-CAN aircraft campaign. BrC Abs_{405} was directly measured during MOONLIGHT, while absorption from BC was subtracted from the 405-nm PAS signal during WE-CAN (*SI Appendix*, Sect. 1.1.1). The FIGAERO-CIMS provided quantitative molecular-level measurements of particulate nitrophenols, which allowed for calibration of real-time particulate nitrophenol parent tracer ions measured in the AMS and thus a direct connection to observations of particulate nitrophenols and BrC Abs_{405} in the wildfire plumes studied during WE-CAN.

Fig. 5*A* shows the strong correlation between the sum of particulate nitrophenols ($C_6H_5NO_3$ and $C_6H_5NO_4$) measured using the FIGAERO-CIMS versus the corresponding tracer ions measured by the AMS during phenol and catechol oxidation experiments. This relationship shows that the AMS tracer ions can provide an estimate of the mass concentration of the sum of $C_6H_5NO_3$ and $C_6H_5NO_4$ in ambient OA. The two compounds were summed due to the fact that nitrocatechol fragments into both $C_6H_5NO_3^+$ and $C_6H_5NO_4^+$ ions in the AMS, and the particulate concentrations of $C_6H_5NO_4$ measured by the FIGAERO-CIMS were always much larger than $C_6H_5NO_3$, so it was not possible to independently determine their individual relationships between FIGAERO-CIMS and AMS measurements. The time series of FIGAERO-CIMS particulate nitrophenolic compounds, BrC Abs_{405}, and select AMS tracer ions are shown in the *SI Appendix*, Fig. S8 and indicate that this interpretation extends to other nitrophenolic compounds as well (*SI Appendix*, Fig. S9).

We found that BrC Abs_{405} was correlated with the sum of particulate nitrophenolic compounds measured with the FIGAERO-CIMS (*SI Appendix*, Fig. S10) and with the corresponding tracer ions in the AMS (Fig. 5*B*). Nitrophenolic compounds were the dominant contributors to the initial SOA mass measured in the chamber experiments but decreased as a fraction over time with correlated changes in BrC Abs_{405}, and thus we assume they are responsible for the majority of measured light absorption. Under this assumption, the nitrophenolic compounds (predominantly nitrocatechol) have an effective absorption cross-section of 9.0×10^{-18} cm^2 per molecule (*SI Appendix*, Fig. S10), which is similar to values expected for particulate nitrophenolics (54, 55).

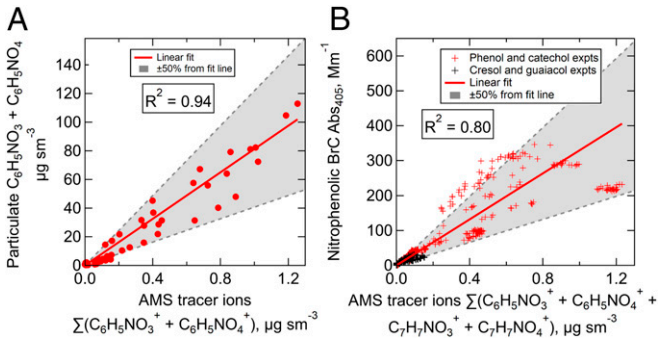

Fig. 5. (*A*) Sum of particulate $C_6H_5NO_3$ and $C_6H_5NO_4$ measured with FIGAERO-CIMS versus the corresponding tracer ions measured with the AMS. The linear fit indicates particulate nitrophenolic mass ($\mu g\ sm^{-3}$) = 81.3 × AMS tracer ion mass ($\mu g\ sm^{-3}$). (*B*) BrC Abs_{405} measured using the PAS, as a function of the sum of AMS tracer ion mass ($C_6H_5NO_3^+$ and $C_6H_5NO_4^+$ during phenol and catechol oxidation experiments, or $C_7H_7NO_3^+$ and $C_7H_7NO_4^+$ during cresol and guaiacol oxidation experiments). The linear fit indicates nitrophenolic BrC Abs_{405} (Mm^{-1}) = 329 × AMS tracer ion mass ($\mu g\ sm^{-3}$). To account for possible sources of error such as isomeric variations or differences in particle transmission across different experiments, ±50% error bars are included in both *A* and *B* to empirically bound the data.

The AMS tracer ions quantified during the MOONLIGHT chamber experiments were also quantified during WE-CAN wildfire plume measurements. Thus, we can apply the relationships of particulate nitrophenolic mass and BrC Abs_{405} as a function of AMS tracer ions (Fig. 5 *A* and *B*) to the wildfire measurements to estimate particulate nitrophenolic mass and their contributions to BrC Abs_{405} in the wildfire plumes. Shown in Fig. 6 is a summary of gas-phase phenolics, estimated particulate nitrophenolics, OA, and BrC Abs_{405} observations from nine wildfires during WE-CAN with coherent plumes for which physical age could be estimated. Each of these plumes were sampled at a minimum of three different physical ages. The sum of phenolics exhibited a clear decay, as indicated in Fig. 3 and *SI Appendix*, Fig. S4 (*SI Appendix*). Both OA and BrC Abs_{405} NEMRs remain roughly constant over the range of plume ages, although some variability within and across plumes is evident. As explained above in *Insights into Dilution-Driven BBPOA Evaporation and BBSOA Formation*, this view conceals the balance between dilution-driven evaporation and subsequent secondary formation. Using the MOONLIGHT campaign relationships with the empirical ±50% error bars shown in Fig. 5, we estimate that particulate nitrophenolic compounds, dominated by components with molecular compositions of nitrophenol and nitrocatechol, comprise an average of 9 ± 5 $\mu g\ sm^{-3}\ ppm^{-1}$ OA NEMR (with an SD of ±3 $\mu g\ sm^{-3}\ ppm^{-1}$ due to variability between different fires) and can explain an average of 36 ± 18 $Mm^{-1}\ ppm^{-1}$ BrC Abs_{405} NEMR (SD of ±13 $Mm^{-1}\ ppm^{-1}$ between fires). These values correspond to an average of 4 ± 2% of OA and 29 ± 15% of BrC Abs_{405} NEMRs (with SDs between fires of ±1 and ±12%, respectively). Thus, while accounting for only a small fraction of total OA, phenolic-derived OA makes an outsized contribution to BrC Abs_{405}, reaching as much as 40% or more in some wildfire plumes. This is consistent with previous literature illustrating the outsized role in BrC absorption of compounds with relatively small mass concentrations such as nitrophenolics (e.g., refs. 33, 56, 57). Given the depletion of particulate nitrophenols and BrC Abs_{405} in the chamber experiments with extended oxidative aging, this molecular connection could therefore explain a significant fraction of the apparent decreases of BrC in aged BB plumes through the continued oxidation of nitrophenols into products with fewer or weaker chromophores. As shown in *SI Appendix*, Fig. S11, a modest correlation is found between the evolution of BrC Abs_{405} NEMR and the evolution of the estimated contribution of nitrophenols to BrC Abs_{405}, although other subsets of BrC are likely contributing as well.

Conclusions

We present quantitative measurements of the evolution of BBSOA and sBrC Abs_{405} in wildfire plumes, illustrating that the balance of dilution-driven BBPOA evaporation and subsequent BBSOA formation is not merely serendipitous but a result of evaporated BBPOA being the dominant source of BBSOA. We find that phenolic compounds and their oxidation products are substantial contributors to total BrC Abs_{405} in western US wildfire plumes, despite less contribution to total OA mass. Total phenolic emissions were typically 1 to 3 ppt ppb^{-1}, although this may be an underestimate due to the fast reactivity of some. With a combined analysis of simulation chamber measurements and field data, nitrophenolic compounds were estimated to account for an average of 4 ± 2% of total OA mass but 29 ± 15% of total BrC Abs_{405}.

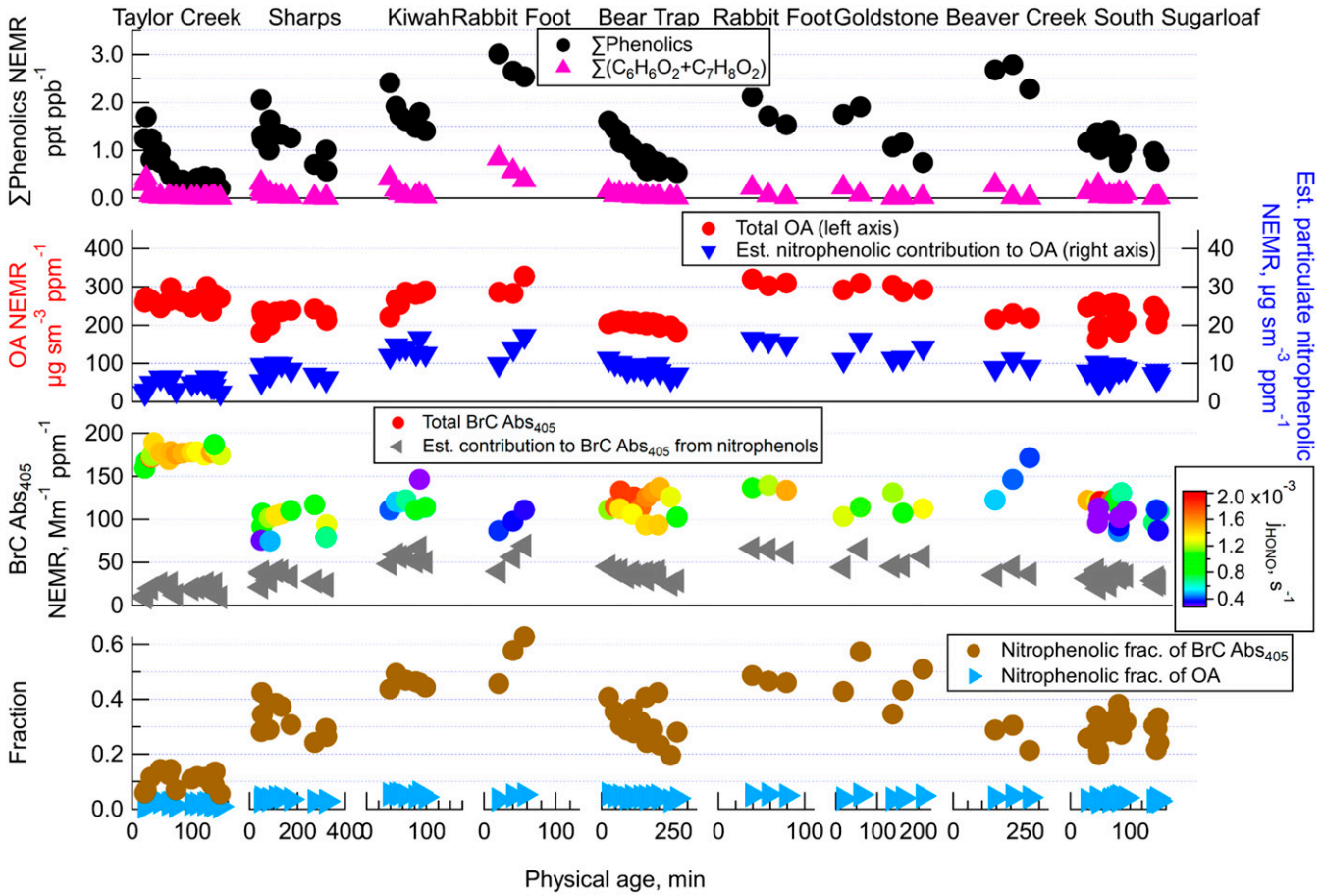

Fig. 6. Evolution of the NEMRs of sum of gas-phase phenolics, OA, BrC Abs_{405}, estimated particulate nitrophenolic mass, and particulate nitrophenolic fractions of total OA and BrC Abs_{405} as a function of physical age for nine distinct wildfire plumes (labeled at top). The BrC Abs_{405} NEMR is colored by j_{HONO} as a proxy for the intensity of photochemistry.

By estimating a dilution factor for each plume transect, we illustrated the competing effects of evaporation of primary OA and BrC versus secondary formation from phenolics and other gases. Our observationally constrained analysis indicates that the oxidation of evaporated BBPOA plays a dominant role in determining aerosol properties, with relatively minor contributions from the oxidation of directly emitted precursor gases in such large wildfires in the western United States. The estimate of BBSOA from emitted vapors is admittedly uncertain, but even after accounting for large potential biases, we find that evaporated BBPOA likely explains at least half of the BBSOA that forms in the first 3 to 6 h of wildfire plume evolution.

Essentially all of the wildfire plume data presented herein were taken during the afternoon hours while photochemistry was active. HONO photolysis was the likely driver of phenolic compound evolution (45), but this source of OH would be inactive during nighttime hours. These measurements leave a substantial gap in our understanding of the evolution of phenolic compounds during nighttime hours. Nitrate radical chemistry would likely play an important role in such plumes. Our MOONLIGHT chamber experiments suggest a strong connection between NO_3 oxidation of phenolic compounds and production of BrC Abs_{405} consistent with past studies. Thus, future work, such as nighttime flights or nighttime ground-based stationary/mobile laboratory measurements, should focus on this question and on how the emission rates of phenolic compounds relative to CO may change as the fires tend to become less active during nighttime.

Materials and Methods

Descriptions of the WE-CAN and MOONLIGHT campaigns and further details of instrument operation, calibration, and analysis and methods of calculating NEMRs and the dilution factor can be found in *SI Appendix*, along with all SI figures and tables referenced throughout the article.

Data Availability. WE-CAN data from the I^- CIMS have been deposited in the NCAR Earth Observing Laboratory data archive (https://doi.org/10.26023/DADR-F5C2-WM06 and https://doi.org/10.26023/27YS-3XAN-7A0W). Other data from WE-CAN can be found at https://data.eol.ucar.edu/project/WE-CAN or in Dataset S1. Data from the MOONLIGHT campaign are included in Dataset S1.

ACKNOWLEDGMENTS. We sincerely thank everyone involved in the planning and operation of the 2018 WE-CAN campaign and 2019 MOONLIGHT campaign. B.B.P., Q.P., C.D.F., B.H.L., and J.A.T. were supported by US NSF Grant AGS-1652688 and National Oceanic and Atmospheric Administration (NOAA) Grant NA17OAR4310012). L.A.G., M.A.P., S.M.K., and D.K.F. were supported by NOAA Grant NA17OAR4310010. R.P.P., Y.S., and S.M.M. acknowledge support from US Environmental Protection Agency Grant R835883. This research was supported in part by US NSF Grants AGS-1650786 and AGS-1650275. This material is based upon work supported by the NCAR, which is a major facility sponsored by the US NSF under Cooperative Agreement 1852977. The data were collected using NSF's Lower Atmosphere Observing Facilities, which are managed and operated by NCAR's Earth Observing Laboratory. The operational and scientific support from NCAR's Earth Observing Laboratory and Research Aircraft Facility is gratefully acknowledged.

1. M. O. Andreae, P. Merlet, Emission of trace gases and aerosols from biomass burning. *Global Biogeochem. Cycles* **15**, 955–966 (2001).
2. S. K. Akagi *et al*., Emission factors for open and domestic biomass burning for use in atmospheric models. *Atmos. Chem. Phys.* **11**, 4039–4072 (2011).
3. A. F. Bouwman *et al*., A global high-resolution emission inventory for ammonia. *Global Biogeochem. Cycles* **11**, 561–587 (1997).
4. D. S. Lee *et al*., Estimations of global NOx emissions and their uncertainties [Review]. *Atmos. Environ.* **31**, 1735–1749 (1997).
5. K. B. Benedict *et al*., Enhanced concentrations of reactive nitrogen species in wildfire smoke. *Atmos. Environ.* **148**, 8–15 (2017).
6. D. A. Hegg, L. F. Radke, P. V. Hobbs, R. A. Rasmussen, P. J. Riggan, Emissions of some trace gases from biomass fires. *J. Geophys. Res.* **95**, 5669–5675 (1990).
7. T. C. Bond *et al*., A technology-based global inventory of black and organic carbon emissions from combustion. *J. Geophys. Res.* **109**, D14203 (2004).
8. A. P. Grieshop, J. M. Logue, N. M. Donahue, A. L. Robinson, Laboratory investigation of photochemical oxidation of organic aerosol from wood fires 1: Measurement and simulation of organic aerosol evolution. *Atmos. Chem. Phys.* **9**, 1263–1277 (2009).
9. C. J. Hennigan *et al*., Chemical and physical transformations of organic aerosol from the photo-oxidation of open biomass burning emissions in an environmental chamber. *Atmos. Chem. Phys.* **11**, 7669–7686 (2011).
10. A. M. Ortega *et al*., Secondary organic aerosol formation and primary organic aerosol oxidation from biomass-burning smoke in a flow reactor during FLAME-3. *Atmos. Chem. Phys.* **13**, 11551–11571 (2013).
11. E. A. Bruns *et al*., Identification of significant precursor gases of secondary organic aerosols from residential wood combustion. *Sci. Rep.* **6**, 27881 (2016).
12. G. Capes *et al*., Secondary organic aerosol from biogenic VOCs over West Africa during AMMA. *Atmos. Chem. Phys.* **9**, 3841–3850 (2009).
13. R. J. Yokelson *et al*., Emissions from biomass burning in the Yucatan. *Atmos. Chem. Phys.* **9**, 5785–5812 (2009).
14. M. J. Cubison *et al*., Effects of aging on organic aerosol from open biomass burning smoke in aircraft and laboratory studies. *Atmos. Chem. Phys.* **11**, 12049–12064 (2011).
15. S. K. Akagi *et al*., Evolution of trace gases and particles emitted by a chaparral fire in California. *Atmos. Chem. Phys.* **12**, 1397–1421 (2012).
16. H. Forrister *et al*., Evolution of brown carbon in wildfire plumes. *Geophys. Res. Lett.* **42**, 4623–4630 (2015).
17. L. A. Garofalo *et al*., Emission and evolution of submicron organic aerosol in smoke from wildfires in the western United States. *ACS Earth Space Chem.* **3**, 1237–1247 (2019).
18. A. A. May *et al*., Observations and analysis of organic aerosol evolution in some prescribed fire smoke plumes. *Atmos. Chem. Phys.* **15**, 6323–6335 (2015).
19. S. Zhou *et al*., Regional influence of wildfires on aerosol chemistry in the western US and insights into atmospheric aging of biomass burning organic aerosol. *Atmos. Chem. Phys.* **17**, 2477–2493 (2017).
20. Q. Bian *et al*., Secondary organic aerosol formation in biomass-burning plumes: Theoretical analysis of lab studies and ambient plumes. *Atmos. Chem. Phys.* **17**, 5459–5475 (2017).
21. A. L. Hodshire *et al*., More than emissions and chemistry: Fire size, dilution, and background aerosol also greatly influence near-field biomass burning aerosol aging. *J. Geophys. Res. Atmos.* **124**, 5589–5611 (2019).
22. L. E. Hatch *et al*., Identification and quantification of gaseous organic compounds emitted from biomass burning using two-dimensional gas chromatography–time-of-flight mass spectrometry. *Atmos. Chem. Phys.* **15**, 1865–1899 (2015).
23. A. T. Ahern *et al*., Production of secondary organic aerosol during aging of biomass burning smoke from fresh fuels and its relationship to VOC precursors. *J. Geophys. Res. Atmos.* **124**, 3583–3606 (2019).
24. G. Stefenelli *et al*., Secondary organic aerosol formation from smoldering and flaming combustion of biomass: A box model parametrization based on volatility basis set. *Atmos. Chem. Phys.* **19**, 11461–11484 (2019).
25. A. Akherati *et al*., Oxygenated aromatic compounds are important precursors of secondary organic aerosol in biomass-burning emissions. *Environ. Sci. Technol.* **54**, 8568–8579 (2020).
26. Y. Feng, V. Ramanathan, V. R. Kotamarthi, Brown carbon: A significant atmospheric absorber of solar radiation? *Atmos. Chem. Phys.* **13**, 8607–8621 (2013).
27. J. Liu *et al*., Brown carbon aerosol in the North American continental troposphere: Sources, abundance, and radiative forcing. *Atmos. Chem. Phys.* **15**, 7841–7858 (2015).
28. R. A. Washenfelder *et al*., Biomass burning dominates brown carbon absorption in the rural southeastern United States. *Geophys. Res. Lett.* **42**, 653–664 (2015).
29. R. Saleh *et al*., Absorptivity of brown carbon in fresh and photo-chemically aged biomass-burning emissions. *Atmos. Chem. Phys.* **13**, 7683–7693 (2013).
30. A. Laskin, J. Laskin, S. A. Nizkorodov, Chemistry of atmospheric brown carbon. *Chem. Rev.* **115**, 4335–4382 (2015).
31. M. Claeys *et al*., Chemical characterisation of humic-like substances from urban, rural and tropical biomass burning environments using liquid chromatography with UV/vis photodiode array detection and electrospray ionisation mass spectrometry. *Environ. Chem.* **9**, 273–284 (2012).
32. Y. Desyaterik *et al*., Speciation of "brown" carbon in cloud water impacted by agricultural biomass burning in eastern China. *J. Geophys. Res. Atmos.* **118**, 7389–7399 (2013).
33. C. Mohr *et al*., Contribution of nitrated phenols to wood burning brown carbon light absorption in Detling, United Kingdom during winter time. *Environ. Sci. Technol.* **47**, 6316–6324 (2013).
34. P. Lin *et al*., Molecular chemistry of atmospheric Brown carbon inferred from a Nationwide biomass burning event. *Environ. Sci. Technol.* **51**, 11561–11570 (2017).
35. X. Liu *et al*., Agricultural fires in the southeastern U.S. during SEAC4RS: Emissions of trace gases and particles and evolution of ozone, reactive nitrogen, and organic aerosol. *J. Geophys. Res. Atmos.* **121**, 7383–7414 (2016).
36. M. Zhong, M. Jang, Dynamic light absorption of biomass-burning organic carbon photochemically aged under natural sunlight. *Atmos. Chem. Phys.* **14**, 1517–1525 (2014).
37. R. Zhao *et al*., Photochemical processing of aqueous atmospheric brown carbon. *Atmos. Chem. Phys.* **15**, 6087–6100 (2015).
38. J. F. Pankow, An absorption model of gas/particle partitioning of organic compounds in the atmosphere. *Atmos. Environ.* **28**, 185–188 (1994).
39. N. M. Donahue, A. L. Robinson, C. O. Stanier, S. N. Pandis, Coupled partitioning, dilution, and chemical aging of semivolatile organics. *Environ. Sci. Technol.* **40**, 2635–2643 (2006).
40. A. L. Robinson *et al*., Rethinking organic aerosols: Semivolatile emissions and photochemical aging. *Science* **315**, 1259–1262 (2007).
41. X. Liu *et al*., Airborne measurements of western U.S. wildfire emissions: Comparison with prescribed burning and air quality implications. *J. Geophys. Res. Atmos.* **122**, 6108–6129 (2017).
42. L. T. Fleming *et al*., Molecular composition and photochemical lifetimes of brown carbon chromophores in biomass burning organic aerosol. *Atmos. Chem. Phys.* **20**, 1105–1129 (2020).
43. K. Sekimoto *et al*., High- and low-temperature pyrolysis profiles describe volatile organic compound emissions from western US wildfire fuels. *Atmos. Chem. Phys.* **18**, 9263–9281 (2018).
44. A. R. Koss *et al*., Non-methane organic gas emissions from biomass burning: Identification, quantification, and emission factors from PTR-ToF during the FIREX 2016 laboratory experiment. *Atmos. Chem. Phys.* **18**, 3299–3319 (2018).
45. Q. Peng *et al*., HONO emissions from western U.S. wildfires provide dominant radical source in fresh wildfire smoke. *Environ. Sci. Technol.* **54**, 5954–5963 (2020).
46. P. Veres *et al*., Measurements of gas-phase inorganic and organic acids from biomass fires by negative-ion proton-transfer chemical-ionization mass spectrometry. *J. Geophys. Res.* **115**, D23302 (2010).
47. R. J. Yokelson *et al*., Coupling field and laboratory measurements to estimate the emission factors of identified and unidentified trace gases for prescribed fires. *Atmos. Chem. Phys.* **13**, 89–116 (2013).
48. E. A. Bruns *et al*., Characterization of gas-phase organics using proton transfer reaction time-of-flight mass spectrometry: Fresh and aged residential wood combustion emissions. *Atmos. Chem. Phys.* **17**, 705–720 (2017).
49. L. E. Hatch *et al*., Multi-instrument comparison and compilation of non-methane organic gas emissions from biomass burning and implications for smoke-derived secondary organic aerosol precursors. *Atmos. Chem. Phys.* **17**, 1471–1489 (2017).
50. X. Zhang *et al*., Influence of vapor wall loss in laboratory chambers on yields of secondary organic aerosol. *Proc. Natl. Acad. Sci. U.S.A.* **111**, 5802–5807 (2014).
51. X. Liu *et al*., Effects of gas–wall interactions on measurements of semivolatile compounds and small polar molecules. *Atmos. Meas. Tech.* **12**, 3137–3149 (2019).
52. B. B. Palm, X. Liu, J. L. Jimenez, J. A. Thornton, Performance of a new coaxial ion–molecule reaction region for low-pressure chemical ionization mass spectrometry with reduced instrument wall interactions. *Atmos. Meas. Tech.* **12**, 5829–5844 (2019).
53. F. D. Lopez-Hilfiker *et al*., A novel method for online analysis of gas and particle composition: Description and evaluation of a filter inlet for gases and AEROsols (FIGAERO). *Atmos. Meas. Tech.* **7**, 983–1001 (2014).
54. J. Chen, J. C. Wenger, D. S. Venables, Near-ultraviolet absorption cross sections of nitrophenols and their potential influence on tropospheric oxidation capacity. *J. Phys. Chem. A* **115**, 12235–12242 (2011).
55. R. Z. Hinrichs, P. Buczek, J. J. Trivedi, Solar absorption by aerosol-bound nitrophenols compared to aqueous and gaseous nitrophenols. *Environ. Sci. Technol.* **50**, 5661–5667 (2016).
56. W. Yuan *et al*., Characterization of the light-absorbing properties, chromophore composition and sources of brown carbon aerosol in Xi'an, northwestern China. *Atmos. Chem. Phys.* **20**, 5129–5144 (2020).
57. M. Teich *et al*., Contributions of nitrated aromatic compounds to the light absorption of water-soluble and particulate brown carbon in different atmospheric environments in Germany and China. *Atmos. Chem. Phys.* **17**, 1653–1672 (2017).